HHS Public Access

Author manuscript

Mol Pharm. Author manuscript; available in PMC 2019 April 02.

Published in final edited form as:

Mol Pharm. 2018 April 02; 15(4): 1627–1634. doi:10.1021/acs.molpharmaceut.7b01168.

Noninvasive Trafficking of Brentuximab Vedotin and PET Imaging of CD30 in Lung Cancer Murine Models

Lei Kang[†,‡,§], **Dawei Jiang**[‡,∥,§], **Emily B. Ehlerding**[⊥], **Todd E. Barnhart**[⊥], **Dalong Ni**[‡], **Jonathan W. Engle**[⊥], **Rongfu Wang**[†], **Peng Huang**[*,∥], **Xiaojie Xu**[*,#], and **Weibo Cai**[*,‡,⊥,¶]

[†]Department of Nuclear Medicine, Peking University First Hospital, Beijing 100034, China

[‡]Department of Radiology, University of Wisconsin—Madison, Madison, Wisconsin 53705, United States

[∥]Guangdong Key Laboratory for Biomedical Measurements and Ultrasound Imaging, Laboratory of Evolutionary Theranostics, School of Biomedical Engineering, Health Science Center, Shenzhen University, Shenzhen 518060, China

[⊥]Department of Medical Physics, University of Wisconsin—Madison, Madison, Wisconsin 53705, United States

[#]Department of Medical Molecular Biology, Beijing Institute of Biotechnology, Beijing 100850, China

[¶]University of Wisconsin Carbone Cancer Center, Madison, Wisconsin 53705, United States

Abstract

CD30 has been considered a unique diagnostic and therapeutic target for CD30-positive lymphomas and some lung diseases. Additionally, CD30 has shown high expression in clinical lung cancer samples. In this study, ^{89}Zr-radiolabeled brentuximab vedotin (BV) was developed for *in vivo* tracking of BV and imaging CD30 expression in lung cancer models via conjugation with desferrioxamine (Df). CD30 expression in three lung cancer cell lines (H460, H358, and A549) was quantified by Western blot. Flow cytometry and saturation binding assays were used to evaluate the binding capabilities of the tracer *in vitro*. After longitudinal positron emission tomography (PET) imaging and quantitative analysis were performed, *ex vivo* biodistribution and histological studies were used to verify PET results. Finally, dosimetric extrapolation of murine

[*]**Corresponding Authors:** W.C.: Room 7137, 1111 Highland Ave, Madison, WI 53705- 2275, USA. wcai@uwhealth.org. Phone: 608-262-1749. Fax: 608-265-0614.; X.X.: Department of Medical Molecular Biology, Beijing Institute of Biotechnology, 27 Tai-Ping Rd, Beijing, 100850, China. miraclexxj@126.com. Phone: 86-10-6693-1830. Fax: 86-10-6824-8045.; P.H.: Nanhai Ave 3688, Guangdong Key Laboratory for Biomedical Measurements and Ultrasound Imaging, Laboratory of Evolutionary Theranostics, School of Biomedical Engineering, Health Science Center, Shenzhen University, Shenzhen, Guangzhou, 518060, China. peng.huang@szu.edu.cn. Phone: 86-755-86671911.

[§]**Author Contributions**

L.K. and D.J. contributed equally to this work.

ORCID

Dawei Jiang: 0000-0002-4072-0075

Dalong Ni: 0000-0001-6679-5414

Peng Huang: 0000-0003-3651-7813

Weibo Cai: 0000-0003-4641-0833

Notes

The authors declare no competing financial interest.

data to humans was performed. At the cellular level, CD30 was found to be expressed on H460 and A549 cells with the highest and lowest levels of expression, respectively. Both Df-BV and ^{89}Zr-Df-BV displayed high binding affinity to H460 cells. PET images and their quantification verified that BV accumulated in H460 tumor models (9.93 ± 2.70% ID/g at 24 h after injection; n = 4) at the highest level, followed by H358 and A549 tumors (8.05 ± 2.43 and 5.00 ± 1.56% ID/g; n = 4). The nonspecific ^{89}Zr-labeled IgG showed a low tumor uptake of 5.2 ± 1.0% ID/g for H460 models. *Ex vivo* biodistribution and fluorescence immunohistochemistry also corroborated these findings. Dosimetric results displayed safe dose estimations. Therefore, ^{89}Zr-Df- BV provides a potential agent for evaluating CD30 expression noninvasively in lung cancer, and also for imaging of brentuximab vedotin for better understanding of its pharmacokinetics.

Graphical abstract

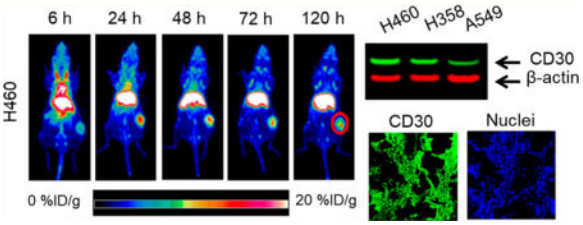

Keywords

brentuximab vedotin; CD30; positron emission tomography (PET); Zr-89; lung cancer

INTRODUCTION

Cluster determinant 30 (CD30) is a 120 kDa transmembrane glycoprotein and recognized as the eighth member of the tumor necrosis factor receptor superfamily (TNFRSF8).[1] It interacts with TRAF2 or TRAF5 proteins to activate the nuclear factor kappa B (NF-κB), and leads to cellular propagation and differentiation.[2] CD30 is additionally expressed by T- or B-cell origin lymphoid cells in Hodgkin's lymphoma, large cell anaplastic lymphoma, and some large B-cell lymphomas, and is thus considered a unique diagnostic and therapeutic target for these diseases, among others.[1–3] Differential expression of CD30 has also been reported on the membranes of decidual cells, mesothelial cells, myoepithelial cells, NK cells, thymic cells, and macrophages.[4] In addition to lymphomas, embryonal carcinoma and malignant mesothelioma are also CD30-positive such that it is of potential diagnostic and therapeutic value.[5,6] Other cancers have been reported as CD30-positive, such as seminomas,[7] melanoma,[8] nasopharyngeal carcinoma,[9] and cavernous and spindle cell hemangiomas.[10] In the area of lung diseases, the CD30 ligand was reported as a lung cancer biomarker and observed to be upregulated in lung cancer serum[11] and supports lung inflammation.[12]

Based on the critical role of CD30 in malignant lymphomas, several monoclonal antibodies (mAbs) targeting CD30 have been developed for clinical use. Two important first generation anti-CD30 antibodies are chimeric mAb SGN-30 (also known as cAC10) and MDX-060 (also named 5F11).[13] SGN-30 is constructed from the variable regions of a murine anti-

CD30 mAb (named AC10) and human heavy and light chain constant regions.[14] MDX-060 is an intact anti-CD30 human G1κ IgG mAb.[15] Because these mAbs showed low response rates and unpredictable side effects in clinical trials, some modified anti-CD30 mAbs were developed to improve their treatment efficiency. Among them, antibody–drug conjugates (ADCs) have shown obvious enhanced antitumor activity.[16]

Brentuximab vedotin (BV, Seattle Genetics, Adcetris), also named SGN-35, is one of the most successful ADCs. It is composed of SGN-30 attached via an enzyme-cleavable dipeptide linker to an antitubulin agent, monomethyl auristatin E (MMAE).[17] After binding to CD30, BV is internalized and transported to lysosomes, and MMAE is released through proteolytic cleavage. MMAE binds to tubulin and disrupts the microtubule network within the cell, causing arrest of the cell cycle and apoptotic cell death.[18] Additional means of tumor cell destruction are contributed by antibody-dependent cellular phagocytosis, bystander effects in the tumor microenvironment, and immunogenic cell death.[17,19] Because BV revealed high response rates as a single agent for treatment, it was speedily approved for CD30-positive relapsed Hodgkin lymphoma and relapsed systemic anaplastic large-cell lymphoma (sALCL) by the FDA.[20] Therefore, the trafficking of ADCs and monitoring of their therapeutic effect *in vivo* are important for understanding the effects of lymphoma treatment.

In vivo tracking of mAbs enables the visualization of tumor targeting and estimation of the dose delivered to off-target tissues. Positron emission tomography (PET) imaging is commonly used in the clinic for tumor detection and therapeutic efficacy monitoring.[21–23] ImmunoPET combines the high specificity and selectivity of mAbs with the high resolution and quantitative aspects of PET. Therefore, immunoPET is an ideal imaging modality for tumor detection.[22] Compared with short-lived PET radionuclides such as ^{18}F($t_{1/2}$ = 108 min) or ^{68}Ga ($t_{1/2}$ = 68 min), ^{89}Zr ($t_{1/2}$ = 78.4 h) is highly suitable for imaging intact mAbs which typically need up to 4 days to realize optimal tumor-to-nontumor ratios.[22]

One previous report used a ^{89}Zr-labeled murine mAb (AC10) for immunoPET imaging of CD30 in lymphoma models.[24] Although AC10 displays high and specific binding affinity to CD30, the major limitation of murine mAbs is the immunogenicity of the foreign protein, which might induce adverse effects and loss of efficacy.[13] The anti-CD30 chimeric mAb SGN-30, the native antibody component of brentuximab vedotin, is safer to use in humans. Thus, far, no studies have been reported on PET imaging using radiolabeled BV or SGN-30. Moreover, the *in vivo* distribution of BV should be further clarified to determine the biological impact of conjugation of MMAE on the binding ability to CD30. Therefore, we radiolabeled BV with ^{89}Zr for tracking BV and imaging CD30 expression noninvasively in three lung cancer models. This study enables visualization of the dynamic distribution of brentuximab vedotin and validates radiolabeled brentuximab vedotin for immunoPET imaging of CD30 *in vivo* for possible future clinical application.

EXPERIMENTAL SECTION

Cell Culture

Three human lung cancer cell lines (H460, H358, and A549) were purchased from the American Type Culture Collection (ATCC, USA). Cells were cultured in RPMI 1640 medium with 10% fetal bovine serum (FBS; Thermo Fisher Scientific, USA) and 1% penicillin–streptomycin (Thermo Fisher Scientific, USA) at 37 °C in a humidified incubator with 5% CO_2.

Radiolabeling of Brentuximab Vedotin

For successful radiolabeling of BV with ^{89}Zr, SCN-Bn-deferoxamine (Df, Macrocyclics, USA) was conjugated to the antibody through the exposed lysine residues. This procedure was described previously.[21,22] Briefly, 4 mg of BV (in PBS) was incubated with Df (in DMSO) at a molar ratio of 1:10 (brentuximab vedotin:Df) and reacted at room temperature for 2 h. The pH value was adjusted to 8.5-9.0 by Na_2CO_3. Df-BV was purified by a PD-10 column (GE Healthcare, USA) to remove unreacted Df molecules. By using a PETrace cyclotron (GE Healthcare, USA), ^{89}Zr was produced via proton irradiation of natural yttrium foils.[25] For radiolabeling, 400 μg (100 μg/mCi) of Df-BV was mixed with 74–148 MBq (2–4 mCi) of ^{89}Zr-oxalate in 0.5 mL of 0.5 M HEPES buffer (pH 7.0) for 30 min at 37 °C. ^{89}Zr-Df-BV was purified using a PD-10 column and assayed for radiochemical yield by collecting different parts of elutions. For a nonspecific control, ^{89}Zr-labeled human serum IgG (ThermoFisher Scientific, USA) was used and prepared using the same procedures described above.

Western Blot

Lung cancer cells were lysed with RIPA buffer (Boston BioProducts, USA) supplemented with 1:100 Inhibitor Cocktail (ThermoFisher Scientific, USA) overnight at 4 °C. Protein concentration was measured using the Pierce Coomassie Protein Assay Kit (ThermoFisher Scientific, USA), and 30 μg of total protein was loaded into a 4–12% Bolt Bis-Tris Plus gel (ThermoFisher Scientific, USA), along with the protein marker Chameleon Duo ladder (LI-COR Biosciences, USA). Gels were electrophoresed at 110 mV and 4 °C for 75 min, and, using the iBlot 2 system (ThermoFisher Scientific, USA), proteins were transferred to a nitrocellulose membrane. The membrane was blocked with Odyssey blocking buffer (LI-COR Biosciences, USA) overnight at 4 °C and then incubated with the primary antibodies including mouse anti-human CD30 antibody (1:1500) and rabbit anti-human β-actin antibody (1:2000) for another 12 h at 4 °C. All primary antibodies were purchased from Novus Biologicals (Littleton, CO, USA). After washing with PBS-T (phosphate buffered saline with Tween 20), the membrane was incubated with secondary antibodies (donkey anti-mouse IRDye 800CW and goat anti-rabbit IRDye 680RD; LI-COR, USA) for 1 h at room temperature. The membrane was washed, scanned, and quantitatively analyzed using the Odyssey infrared Imaging System (LI-COR, USA).

Flow Cytometry

The binding of the antibody to CD30 was assessed by flow cytometry in H460, H358, and A549 cells. Cells were harvested, washed with cold PBS, and resuspended in Flow Cytometry Staining Buffer Solution (eBioscience, USA) at a concentration of 1×10^6 cells/mL. Cells were incubated for 60 min on ice with either BV or Df-BV (at 5 or 25 μg/mL) and washed. Cells were then incubated with 3 μg/mL of goat anti-human AF488 secondary antibody (Thermo-Fisher Scientific, USA) for 30 min on ice. After washing, cells were analyzed using a LSRFortessa cytometer (BD Biosciences, USA) and mean fluorescence intensities were quantified using FlowJo (Tree Star, USA).

Saturation Binding Assay

H460 cells were seeded in a 96-well plate at 1×10^5 cells/well, and gradient concentrations of ^{89}Zr-Df-BV in PBS were added to each well (from 0.03–100 nM). 1 μMmol of unlabeled BV was used to evaluate nonspecific binding. Following a 2 h incubation at room temperature, wells were washed three times with PBS, and cells were collected and counted using a gamma counter (PerkinElmer, USA). The total binding and nonspecific binding isotherms were plotted using GraphPad Prism software 7.00 (La Jolla, CA, USA). Saturation binding: one site total and nonspecific binding was used for fitting of the overall binding curve. Saturation binding: one site specific binding was applied for Specific binding curve; and linear regression fitting was used for Nonspecific binding. The equilibrium dissociation constant (K_d), maximum binding (B_{max}) value, and receptor density were calculated.

Animal Models

All animal studies were conducted with approval from the University of Wisconsin Institutional Animal Care and Use Committee. 4- to 6-week-old female athymic mice (Envigo, United Kingdom) were used for subcutaneous tumor implantation. After harvesting, cells were resuspended in Matrigel (Invitrogen, USA) at a concentration of 5×10^6 cells/mL. 200 μL of H460, H358, or A549 lung cancer cells were subcutaneously injected into the lower right flank of each mouse. Mice were monitored for general health and tumor volumes every other day.

PET Imaging and Image Analysis

Tumor-bearing mice ($n = 4$ per group) were intravenously injected with 7.4–11.1 MBq of ^{89}Zr-Df-BV. At 6, 12, 24, 48, 72, 96, and 120 h postinjection of ^{89}Zr-Df-BV or ^{89}Zr-Df-IgG, PET images were acquired using an Inveon microPET/CT (Siemens Medical Solutions, USA). Mice were placed in the prone position in the scanner after anesthesia was induced and maintained with 2% isoflurane. Twenty million coincidence events were acquired per mouse for every static PET emission scan. PET images were reconstructed using the 3D ordered subset expectation maximization (OSEM3D) algorithm. Quantitative region-of-interest (ROI) data were analyzed by the Inveon Acquisition Workplace (Siemens Medical Solutions, USA) and recorded as the percentage of injected dose per gram (% ID/g). Ratios of organ-to-blood were also calculated.

Ex Vivo Biodistribution Studies

Following the 120 h PET scan, mice were euthanized by CO_2 inhalation and their blood and major organs were collected and weighed before the activities were counted using a gamma counter (PerkinElmer, USA). The radioactive uptake was presented as % ID/g (mean ± SD).

Immunofluorescent Staining

Immunofluorescent staining of tumor tissues used procedures previously described.[23] Briefly, tumors were extracted, sectioned, fixed in cold acetone for 30 min, and dried at room temperature for 15 min. After blocking with 2.5% donkey serum at room temperature for 1 h, the slides were incubated overnight at 4 °C with anti-human CD30 (Novus Biologicals, USA) and anti-mouse CD31 (ThermoFisher Scientific, USA) at concentrations of 1:150 and 10 μg/mL, respectively. The sections were then washed and incubated with Cy3-labeled donkey anti-rat and Alexa- Fluor488 labeled goat anti-mouse antibodies (ThermoFisher Scientific, USA) at room temperature for 2 h. After washing, the slides were coverslipped using Vectashield and Fluoro- mount mediums (Novus Biologicals, USA) for fluorescence microscopy with DAPI (Vector Laboratories, USA). Imaging was performed on a Nikon A1R confocal microscope (Nikon Instruments, USA).

Dosimetric Extrapolation

Using PET tracer uptake data from ROI analysis along with biodistribution data of ^{89}Zr-Df-brentuximab vedotin, whole-body and organ doses to an adult human were estimated using OLINDA.[2]

Statistical Analysis

Quantitative data are expressed as mean ± standard deviation (SD). Statistical significance was analyzed using ANOVA. *P*-values less than 0.05 were considered statistically significant.

RESULTS

CD30 Expression in Lung Cancer Cell Lines

Relative expression levels of CD30 in three lung cancer cell lines (H460, H358, and A549) were measured by Western blot analysis. 61.9 kDa bands represented CD30, while 45 kDa bands represented β-actin. H460 and H358 cells were shown to highly express CD30, whereas A549 was found to express CD30 at a much lower level relative to the expression of β-actin (Figure 1a).

Cellular Binding Abilities of BV, Df-BV, and ^{89}Zr-Df- BV

Flow cytometry was performed to validate the cell binding and immunoreactivity of BV toward CD30 expressed on lung cancer cells and to determine the impact that conjugation of the chelator Df would have on BV's binding affinity (Figure 1b). In H460 cells, BV showed high cell binding ability at both concentrations of 5 and 25 μg/mL, which presented as a stronger shift to the right in the fluorescence histograms. H358 cells express a lower level of CD30, and A549 cells express a background level of CD30. Compared to A549 cells

incubated with secondary antibody only, no significant shift was found with cells incubated with BV or Df-BV. Conjugation of the chelator did not affect the interaction between BV and CD30, as there were minimal changes in signal between BV and Df-BV at both concentrations in H460 cells.

After purification with PD-10 columns, the radiolabeling yield of ^{89}Zr-Df-BV was shown to be greater than 85% with a radiochemical purity of over 95%. The affinity of ^{89}Zr-Df-BV for CD30 was determined via a receptor saturation binding assay. The assay calculated K_d as 2.07 ± 1.86 nM in H460 cells. This value suggests a strong binding affinity between ^{89}Zr-Df-BV and CD30. Additionally, the receptor density of CD30 on the surface of H460 cells was found to be 7.4×10^3 receptors/cell.

PET Imaging

Representative maximum intensity projection (MIP) images from H460, H358, and A549 tumor-bearing mice are shown in Figure 2. Quantitative data were obtained from ROI analyses of the tumor, blood (heart), liver, spleen, kidney, and bone (Figure 3a). Additionally, ^{89}Zr-radiolabeled nonspecific IgG was injected into H460 tumor-bearing mice to exclude nonspecificity of the targeted tracer. For H460 tumor-bearing mice, tumors were effectively visualized with high tracer uptake. ^{89}Zr-Df-BV uptake in H460 increased over time from 6.48 ± 0.39% ID/g to 9.93 ± 2.70% ID/g during 24 h and remained around 9% ID/g through 120 h postinjection ($n = 4$). For A549 tumor-bearing mice, tumors showed very low tracer accumulation, which was significantly lower than that in H460 tumors, at up to 5.00 ± 1.56% ID/g at 72 h postinjection ($n = 4$, $p < 0.05$ when compared with the H460 group). Concordantly, H358 tumors also demonstrated high tracer uptake with a maximum of 8.05 ± 2.43% ID/g at 48 h postinjection ($n = 4$). Therefore, ^{89}Zr-Df-BV demonstrated differential signal in tumors with different CD30 expression.

As a nonspecific control probe, ^{89}Zr-Df-IgG showed very low tumor accumulation (5.2 ± tumor-bearing mice. For all three lung cancer models, the liver showed the highest uptake among all main organs, suggesting the main metabolic path of the tracer *in vivo.* After injection of ^{89}Zr-Df-BV, radioactive uptake in the blood, spleen, and kidneys steadily declined in all tumor models, whereas bone uptake remained constantly low. We further measured the ratios of organ-to-blood activity for the H460 model postinjection of ^{89}Zr-Df-BV or ^{89}Zr-Df-IgG (Figure 3b). Tumor-to-blood ratios reached 2.41 ± 0.45 for ^{89}Zr-Df-BV, but only 1.16 ± 0.13 for ^{89}Zr-Df-IgG at 120 h, suggesting its specific distribution in tumor. ^{89}Zr-Df-BV and ^{89}Zr-Df-IgG showed similar organ-to-blood ratios in the spleen, kidney, and bones. Even though the bone-to-blood ratio increased, it was lower than that of the kidney and spleen and below 1 within 120 h.

Biodistribution

After the final imaging time point at 120 h postinjection, mice were euthanized, and the blood, major organs, and tissues were collected for *ex vivo* validation. Biodistribution studies showed similar findings to the PET imaging results (Figure 4). After injection of ^{89}Zr-Df-BV, a statistically significant difference in tumor uptake was found between H460 and A549 or H358 and A549 models ($n = 4$, $p < 0.05$), further corroborating the PET data.

Blood and liver signals also correlated well with the PET data. Maximum uptake was found in the liver. Tumor uptake of ^{89}Zr-Df-IgG in H460 (3.12 ± 1.59% ID/g) was also significantly lower than that of ^{89}Zr-Df-BV (9.19 ± 0.62% ID/g), which suggested that ^{89}Zr-Df-BV had specific tumor binding *in vivo.*

Immunofluorescent Staining of Lung Tumors

Immunofluorescent staining of tumor tissues further verified the in *situ* expression levels of CD30 in lung cancer models. H460 and H358 tumor tissues showed high staining of CD30 with more homogeneous expression of CD30 than A549 tumors (Figure 5). A549 tumors showed near-background levels of staining for CD30. Anti-mouse CD31 staining visualized vessels in the tumor tissues. The CD30 staining intensities correlated with the tumor uptake found in PET imaging analysis, further verifying the ability of ^{89}Zr-Df-BV to visualize CD30 expression noninvasively in lung cancer.

Dosimetry

Utilizing biodistribution and quantitative ROI data of ^{89}Zr-Df-BV, approximate doses to normal organs following administration of ^{89}Zr-Df-BV were calculated. As shown in Figure 6, the liver was the highest uptake organ after administration of ^{89}Zr-Df-BV in lung cancer models. The calculated absorbed doses to the liver were approximately 2.48 ± 0.67 (H460 model), 2.85 ± 0.22 (H358 model), and 3.13 ± 0.29 (A549 model) mGy/MBq. Since the mice in this group received 200 μCi of ^{89}Zr-Df-BV, the estimated doses to the liver were relatively low, at approximately 1.6 Gy.

DISCUSSION

CD30 is upregulated upon T-cell activation and regulates cytotoxic NK and T-cell effector function, as well as thymocyte survival.[27] While CD30 has been recognized as an important marker for lymphomas for quite some time,[17] its role in lung cancer remained obscure. One study showed that the CD30 ligand can be a lung cancer biomarker, upregulated in lung cancer patients' serum.[11] In clinical settings, the need to maximize drug delivery to CD30-positive cancer cells while minimizing nontarget distribution has put forth the development of BV, which consists of a CD30-specific chimeric monoclonal antibody SGN-30 (also named cAC10) and an anti-tubulin drug (MMAE). Previous studies presented CD30 as a potential target for BV treatment in epithelial-type mesothelioma,[6] and BV has allowed for durable responses with moderate adverse effects. Yet, little is known about the biodistribution of BV *in vivo*. For these purposes, we radiolabeled BV via conjugation with Df to investigate its localization *in vivo* and evaluated differential CD30 expression of three lung cancer models using ^{89}Zr-Df-BV.

Even though the biodistribution and metabolism of ADCs can be inferred from studies with antibodies alone, there is also evidence that these characteristics of ADCs may be different from those of pure antibodies.[28] When evaluating the biodistribution of an ADC, longitudinal immunoPET may provide a noninvasive method to show the dynamic transportation of the ADC and the active expression of the target molecule *in vivo*.[29] One previous study used a ^{89}Zr-radiolabeled murine mAb AC10 to image CD30 expression in

murine lymphoma models.[24] However, this murine antibody is different from SGN-30 (or cAC10), the antibody part of brentuximab vedotin. Moreover, the conjugation of drug molecules, such as MMAE, will likely lead to a decreased serum half-life. In this study, heart (blood) uptake of ^{89}Zr-Df-BV dropped more than 50% from 24 to 72 h after injection, while that of ^{89}Zr-Df-AC10 decreased by less than 30% in the previous study. Additionally, the liver uptake of ^{89}Zr-Df-BV in the CD30-positive H460 group maintained at approximately 20% ID/g from 24 to 72 h postinjection in our study, while the liver uptake of ^{89}Zr-Df-AC10 decreased from 15.22 ± 1.71% ID/g to 11.78 ± 2.43% ID/g during the same time period in a CD30-positive lymphoma model. This difference is likely caused by the high liver metabolism of the drug conjugate, which enhanced the hydrophobicity of BV *in vivo*. One preclinical study showed that the major elimination pathway of another ADC (ado-trastuzumab) is also the fecal/biliary route.[28] Similar to other antibody-based agents, the metabolism of ^{89}Zr-Df-BV in our study is thought to take place by hepatic elimination through proteolytic degradation.

One important consideration for accurate PET imaging is that the tracer is adequately stable *in vivo*. As is well-known, free detached ^{89}Zr accumulates in bone. Interestingly, our study showed that the bone uptake of ^{89}Zr-Df-BV remained low (less than 3% ID/g even at 120 h), while ^{89}Zr-Df-AC10 showed obviously increased bone uptake (more than 5% ID/g at the earlier time point of 72 h). The low bone uptake in this study represented the high stability of ^{89}Zr-Df-BV in the body.

Data from immunoPET can allow quantification of the radiation doses to organs-of-interest. In a clinical study, the quantification of blood-pool activity from PET images agreed well with the collected blood sample activity using a ^{89}Zr-radiolabeled mAb.[30] Our study showed that the liver is the major elimination organ for the ADC, so the dosimetry in the liver should be considered for safety concerns. The calculated doses to the liver were approximately 2.48 ± 0.67 (H460 model), 2.85 ± 0.22 (H358 model), and 3.13 ± 0.29 (A549 model) mGy/MBq, which were far less than toxic limits, suggesting its potential safety for future clinical imaging.

Besides immunoPET imaging discussed in our study, radiotherapy using radiolabeled CD30 antibodies or ADCs for targeted treatment of lymphoma has provoked broad interest. Due to the sensitivity of lymphomas to radiotherapy, several preclinical studies have applied ^{131}I-labeled Ki-4 and ^{90}Y-labeled HeFi-1 (anti-CD30 antibodies) for treatment of Hodgkin's lymphoma.[31,32] However, these treatments were only temporarily effective and associated with severe unpredictable hematotoxicity. To maximize treatment effects, radiolabeled ADCs should be rapidly internalized to better transfer cytotoxic drugs into tumor cells, and elicit treatment effects due to the radioisotopes.[16] The excellent targeting ability of BV and its rapid internalization into tumor cells may allow for efficient radiotherapy of CD30-positive lymphoma and other types of cancer.[17] As for the choice of radioisotopes, ^{90}Y is more promising due to its higher beta-energy and longer path length than those of ^{131}I. However, toxicity concerns have limited the widespread use of radioimmunoconjugates.[2] Liver toxicity might be caused by high accumulation of ADCs in the liver. In comparison, smaller antibody fragments such as F(ab′)2 showed lower liver uptake postinjection, as well

as faster blood clearance.[33] At this point, antibody fragments with smaller sizes might be a better choice for radioimmunotherapy to avoid liver toxicity, but further studies are needed.

CONCLUSIONS

In conclusion, brentuximab vedotin was radiolabeled with Zr-89 to enable biodistribution investigations using PET imaging. ^{89}Zr-Df-BV was later found useful for evaluating CD30 expression in lung cancer, and differential CD30 expression was found in three different lung cancer murine models. Therefore, ^{89}Zr-Df-BV may be developed as an imaging agent of CD30 expression in clinical settings, allowing for patient stratification and post-treatment management.

Acknowledgments

This work was supported by the University of Wisconsin—Madison, the National Institutes of Health (NCI P30CA-014520, T32CA009206, T32GM008505), the American Cancer Society (125246-RSG-13-099-01-CCE), the National Natural Science Foundation of China (81672602, 81472589, 31771036, 51703132, 51573096), the Beijing Nova Program (Z141102001814055, Z171100001117024, Z1811000062-18126), the Beijing Capital Special Development Application Program (Z141107002514159), Logistics Scientific Research Project (BWS16J010) and the Basic Research Program of Shenzhen (JCYJ20170412111100742, JCYJ201604220912-38319). All applicable international, national, and/or institutional guidelines for the care and use of animals were followed.

References

1. Muta H, Podack ER. CD30: from basic research to cancer therapy. Immunol Res. 2013; 57(1–3): 151–8. [PubMed: 24233555]
2. Schirrmann T, Steinwand M, Wezler X, Ten Haaf A, Tur MK, Barth S. CD30 as a therapeutic target for lymphoma. BioDrugs. 2014; 28(2):181–209. [PubMed: 24043362]
3. Kumar A, Younes A. Role of CD30 targeting in malignant lymphoma. Curr Treat Options Oncol. 2014; 15(2):210–25. [PubMed: 24570331]
4. Durkop H, Foss HD, Eitelbach F, Anagnostopoulos I, Latza U, Pileri S, Stein H. Expression of the CD30 antigen in nonlymphoid tissues and cells. J Pathol. 2000; 190(5):613–8. [PubMed: 10727988]
5. Pallesen G, Hamilton-Dutoit SJ. Ki-1 (CD30) antigen is regularly expressed by tumor cells of embryonal carcinoma. Am J Pathol. 1988; 133(3):446–50. [PubMed: 2849300]
6. Dabir S, Kresak A, Yang M, Fu P, Wildey G, Dowlati A. CD30 is a potential therapeutic target in malignant mesothelioma. Mol Cancer Ther. 2015; 14(3):740–6. [PubMed: 25589494]
7. Gallegos I, Valdevenito JP, Miranda R, Fernandez C. Immunohistochemistry expression of P53, Ki67, CD30, and CD117 and presence of clinical metastasis at diagnosis of testicular seminoma. Applied immunohistochemistry & molecular morphology: AIMM. 2011; 19(2):147–52. [PubMed: 20881837]
8. Polski JM, Janney CG. Ber-H2 (CD30) immunohistochemical staining in malignant melanoma. Mod Pathol. 1999; 12(9):903–6. [PubMed: 10496599]
9. Kneile JR, Tan G, Suster S, Wakely PE Jr. Expression of CD30 (Ber-H2) in nasopharyngeal carcinoma, undifferentiated type and lymphoepithelioma-like carcinoma. A comparison study with anaplastic large cell lymphoma. Histopathology. 2006; 48(7):855–61. [PubMed: 16722935]
10. Alimchandani M, Wang ZF, Miettinen M. CD30 expression in malignant vascular tumors and its diagnostic and clinical implications: a study of 146 cases. Applied immunohistochemistry & molecular morphology: AIMM. 2014; 22(5):358–62. [PubMed: 24805132]
11. Ostroff RM, Bigbee WL, Franklin W, Gold L, Mehan M, Miller YE, Pass HI, Rom WN, Siegfried JM, Stewart A, Walker JJ, Weissfeld JL, Williams S, Zichi D, Brody EN. Unlocking biomarker discovery: large scale application of aptamer proteomic technology for early detection of lung cancer. PLoS One. 2010; 5(12):e15003. [PubMed: 21170350]

12. Nam SY, Kim YH, Do JS, Choi YH, Seo HJ, Yi HK, Hwang PH, Song CH, Lee HK, Kim JS, Podack ER. CD30 supports lung inflammation. Int Immunol. 2008; 20(2):177–84. [PubMed: 18089617]
13. Carter P. Improving the efficacy of antibody-based cancer therapies. Nat Rev Cancer. 2001; 1(2): 118–29. [PubMed: 11905803]
14. Cerveny CG, Law CL, McCormick RS, Lenox JS, Hamblett KJ, Westendorf LE, Yamane AK, Petroziello JM, Francisco JA, Wahl AF. Signaling via the anti-CD30 mAb SGN-30 sensitizes Hodgkin's disease cells to conventional chemotherapeutics. Leukemia. 2005; 19(9):1648–55. [PubMed: 16049514]
15. Borchmann P, Treml JF, Hansen H, Gottstein C, Schnell R, Staak O, Zhang HF, Davis T, Keler T, Diehl V, Graziano RF, Engert A. The human anti-CD30 antibody 5F11 shows in vitro and in vivo activity against malignant lymphoma. Blood. 2003; 102(10):3737–42. [PubMed: 12881320]
16. Foyil KV, Bartlett NL. Anti-CD30 Antibodies for Hodgkin lymphoma. Curr Hematol Malig Rep. 2010; 5(3):140–7. [PubMed: 20446121]
17. Okeley NM, Miyamoto JB, Zhang X, Sanderson RJ, Benjamin DR, Sievers EL, Senter PD, Alley SC. Intracellular activation of SGN-35, a potent anti-CD30 antibody-drug conjugate. Clin Cancer Res. 2010; 16(3):888–97. [PubMed: 20086002]
18. Hamblett KJ, Senter PD, Chace DF, Sun MM, Lenox J, Cerveny CG, Kissler KM, Bernhardt SX, Kopcha AK, Zabinski RF, Meyer DL, Francisco JA. Effects of drug loading on the antitumor activity of a monoclonal antibody drug conjugate. Clin Cancer Res. 2004; 10(20):7063–70. [PubMed: 15501986]
19. Oflazoglu E, Kissler KM, Sievers EL, Grewal IS, Gerber HP. Combination of the anti-CD30-auristatin-E antibody-drug conjugate (SGN-35) with chemotherapy improves antitumour activity in Hodgkin lymphoma. Br J Haematol. 2008; 142(1):69–73. [PubMed: 18477046]
20. Younes A, Bartlett NL, Leonard JP, Kennedy DA, Lynch CM, Sievers EL, Forero-Torres A. Brentuximab vedotin (SGN-35) for relapsed CD30-positive lymphomas. N Engl J Med. 2010; 363(19):1812–21. [PubMed: 21047225]
21. Hong H, Severin GW, Yang Y, Engle JW, Zhang Y, Barnhart TE, Liu G, Leigh BR, Nickles RJ, Cai W. Positron emission tomography imaging of CD105 expression with 89Zr-Df- TRC105. Eur J Nucl Med Mol Imaging. 2012; 39(1):138–48. [PubMed: 21909753]
22. Ehlerding EB, England CG, Jiang D, Graves SA, Kang L, Lacognata S, Barnhart TE, Cai W. CD38 as a PET Imaging Target in Lung Cancer. Mol Pharmaceutics. 2017; 14(7):2400–2406.
23. England CG, Ehlerding EB, Hernandez R, Rekoske BT, Graves SA, Sun H, Liu G, McNeel DG, Barnhart TE, Cai W. Preclinical Pharmacokinetics and Biodistribution Studies of 89Zr-Labeled Pembrolizumab. J Nucl Med. 2017; 58(1):162–168. [PubMed: 27493273]
24. Rylova SN, Del Pozzo L, Klingeberg C, Tonnesmann R, Illert AL, Meyer PT, Maecke HR, Holland JP. Immuno-PET Imaging of CD30-Positive Lymphoma Using 89Zr-Desferrioxamine-Labeled CD30-Specific AC-10 Antibody. J Nucl Med. 2016; 57(1):96–102. [PubMed: 26514172]
25. Nickles RJ, Avila-Rodriguez MA, Nye JA, Houser EN, Selwyn R G, Schueller MJ, Christian BT, Jensen M. Sustainable production of orphan radionuclides at Wisconsin. Q J Nucl Med Mol Imaging. 2008; 52(2):134–9. [PubMed: 18043541]
26. Stabin MG, Sparks RB, Crowe E. OLINDA/EXM: the second-generation personal computer software for internal dose assessment in nuclear medicine. J Nucl Med. 2005; 46(6):1023–7. [PubMed: 15937315]
27. Bowen MA, Lee RK, Miragliotta G, Nam SY, Podack ER. Structure and expression of murine CD30 and its role in cytokine production. J Immunol. 1996; 156(2):442–9. [PubMed: 8543792]
28. Han TH, Zhao B. Absorption, distribution, metabolism, and excretion considerations for the development of antibody-drug conjugates. Drug Metab Dispos. 2014; 42(11):1914–20. [PubMed: 25048520]
29. Nayak TK, Brechbiel MW. Radioimmunoimaging with longer-lived positron-emitting radionuclides: potentials and challenges. Bioconjugate Chem. 2009; 20(5):825–41.
30. Borjesson PK, Jauw YW, de Bree R, Roos JC, Castelijns JA, Leemans CR, van Dongen GA, Boellaard R. Radiation dosimetry of 89Zr-labeled chimeric monoclonal antibody U36 as used for

immuno-PET in head and neck cancer patients. J Nucl Med. 2009; 50(11):1828–36. [PubMed: 19837762]

31. Schnell R, Dietlein M, Staak JO, Borchmann P, Schomaecker K, Fischer T, Eschner W, Hansen H, Morschhauser F, Schicha H, Diehl V, Raubitschek A, Engert A. Treatment of refractory Hodgkin's lymphoma patients with an iodine-131-labeled murine anti-CD30 monoclonal antibody. J Clin Oncol. 2005; 23(21):4669–78. [PubMed: 16034043]
32. Zhang M, Yao Z, Patel H, Garmestani K, Zhang Z, Talanov VS, Plascjak PS, Goldman CK, Janik JE, Brechbiel MW, Waldmann TA. Effective therapy of murine models of human leukemia and lymphoma with radiolabeled anti-CD30 antibody, HeFi-1. Proc Natl Acad Sci USA. 2007; 104(20):8444–8. [PubMed: 17488826]
33. Lam K, Chan C, Reilly RM. Development and preclinical studies of (64)Cu-NOTA-pertuzumab F(ab′)2 for imaging changes in tumor HER2 expression associated with response to trastuzumab by PET/CT. mAbs. 2017; 9(1):154–164. [PubMed: 27813707]

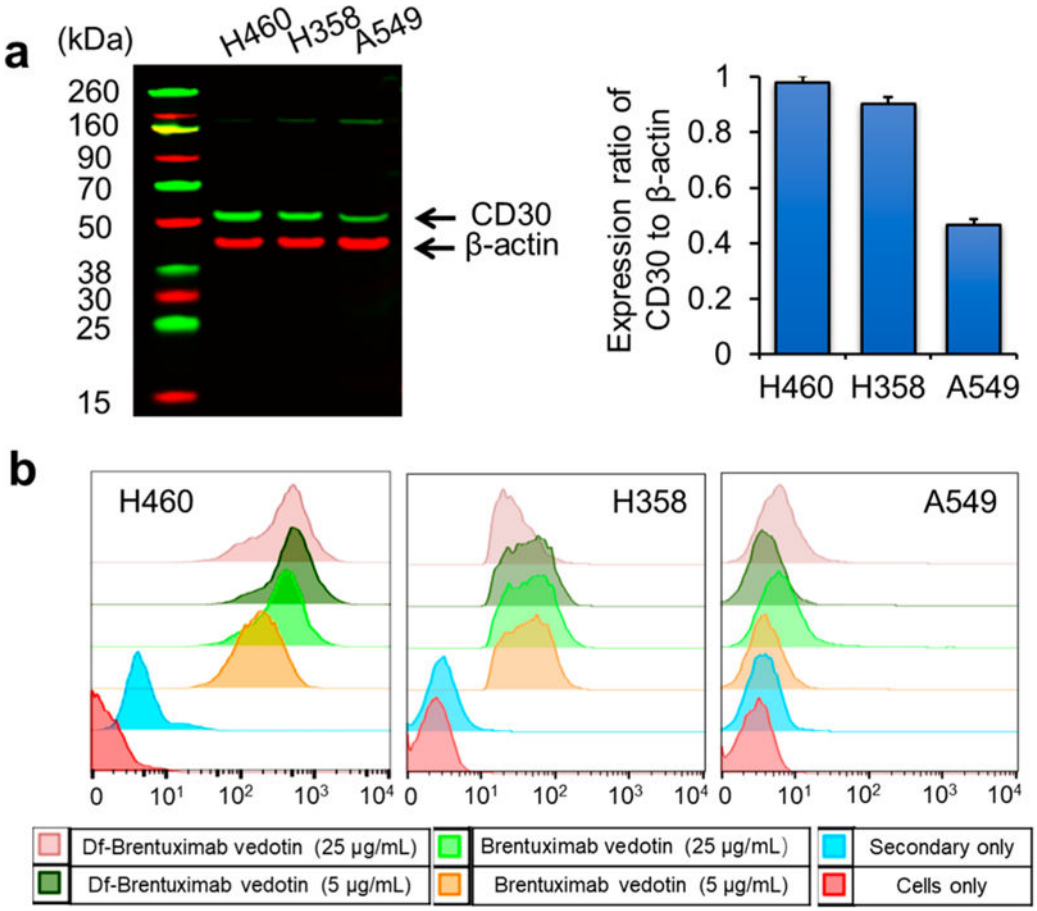

Figure 1.

In *vitro* analysis of CD30 expression and binding ability of BV in H460, H358 and A549 lung cancer cell lines: (a) Western blot analysis; (b) flow cytometry.

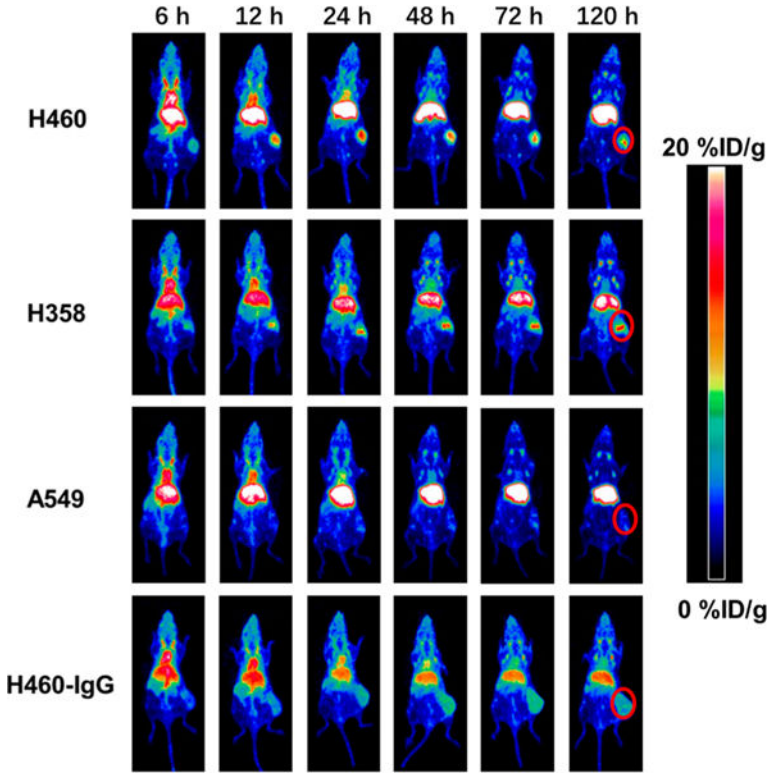

Figure 2.

PET maximum intensity projection (MIP) images of H460, H358, and A549 lung cancer subcutaneous models following injection of ^{89}Zr-Df-BV or ^{89}Zr-Df-IgG. Tumors are shown by red circles.

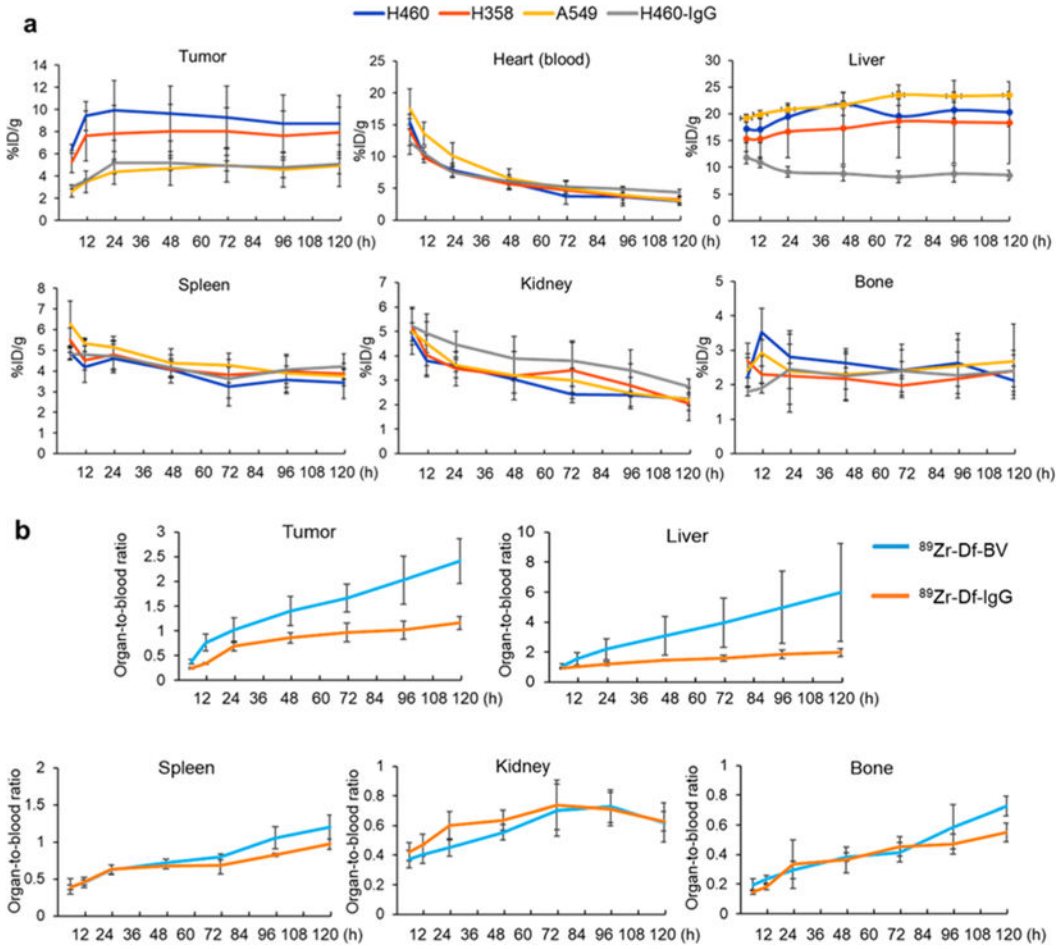

Figure 3.

Quantitative results of PET imaging after injection of ^{89}Zr-Df-BV or ^{89}Zr-Df-IgG in H460, H358, and A549 lung cancer models: (a) radioactivity uptake; (b) organ-to-blood ratios.

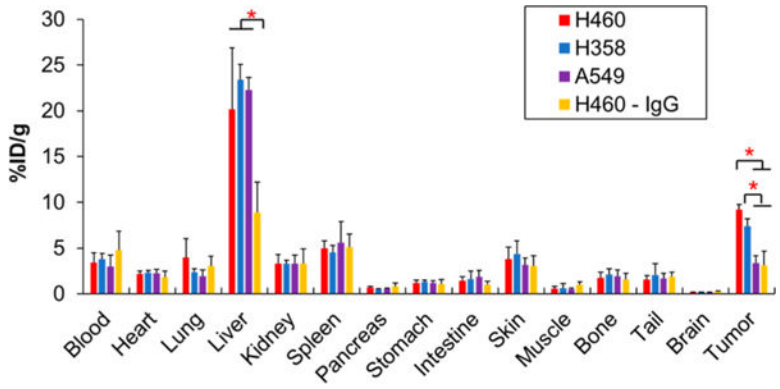

Figure 4.

Ex vivo biodistribution results at 120 h after injection of ^{89}Zr-Df-BV or ^{89}Zr-Df-IgG, which verified the results from PET imaging. *$p < 0.05$.

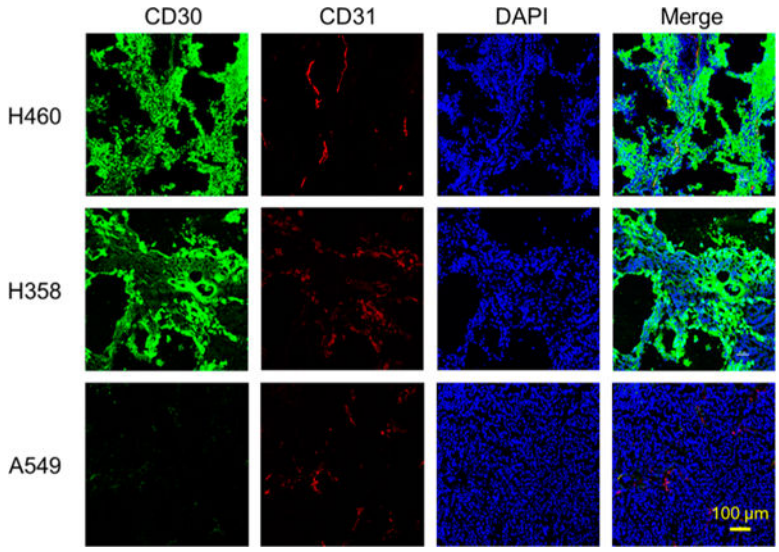

Figure 5.
Immunofluorescent staining of *ex vivo* tumor tissues. Scale bar: 100 μm.

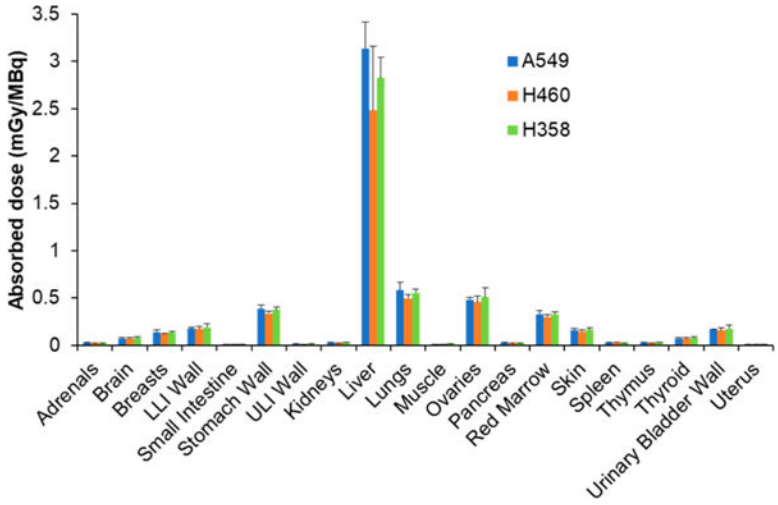

Figure 6.

Estimated doses of ^{89}Zr-Df-BV to normal organs using biodistribution and quantitative ROI data in H460, H358, and A549 lung cancer models, extrapolated to an adult human.